Available online at www.sciencedirect.com
ScienceDirect
Geochimica et Cosmochimica Acta 73 (2009) 2366–2381
Geochimica et Cosmochimica Acta
www.elsevier.com/locate/gca

Experimental studies of equilibrium iron isotope fractionation in ferric aquo–chloro complexes

Pamela S. Hill [a,*], Edwin A. Schauble [a], Anat Shahar [b], Eric Tonui [a], Edward D. Young [a,c]

[a] Department of Earth and Space Sciences, University of California, Los Angeles, CA 90095, USA
[b] Geophyscial Laboratory, Carnegie Institution of Washington, Washington DC 20015, USA
[c] Institute of Geophysics and Planetary Physics, University of California, Los Angeles, CA 90095, USA

Received 7 July 2008; accepted in revised form 22 January 2009; available online 4 February 2009

Abstract

Here we compare new experimental studies with theoretical predictions of equilibrium iron isotopic fractionation among aqueous ferric chloride complexes ($Fe(H_2O)_6^{3+}$, $FeCl(H_2O)_5^{2+}$, $FeCl_2(H_2O)_4^{+}$, $FeCl_3$ $(H_2O)_3$, and $FeCl_4^-$), using the Fe–Cl–H_2O system as a simple, easily-modeled example of the larger variety of iron–ligand compounds, such as chlorides, sulfides, simple organic acids, and siderophores. Isotopic fractionation ($^{56}Fe/^{54}Fe$) among naturally occuring iron-bearing species at Earth surface temperatures (up to ~3‰) is usually attributed to redox effects in the environment. However, theoretical modeling of reduced isotopic partition functions among iron-bearing species in solution also predicts fractionations of similar magnitude due to non-redox changes in speciation (i.e., ligand bond strength and coordination number). In the present study, fractionations are measured in a series of low pH ($[H^+] = 5$ M) solutions of ferric chloride (total Fe = 0.0749 mol/L) at chlorinities ranging from 0.5 to 5.0 mol/L. Advantage is taken of the unique solubility of $FeCl_4^-$ in immiscible diethyl ether to create a separate spectator phase, used to monitor changing fractionation in the aqueous solution. $\Delta^{56}Fe_{aq\text{-}eth} = \delta^{56}Fe$ (total Fe remaining in aqueous phase)$-\delta^{56}Fe$ ($FeCl_4^-$ in ether phase) is determined for each solution via MC-ICPMS analysis.

Both experiments and theoretical calculations of $\Delta^{56}Fe_{aq\text{-}eth}$ show a downward trend with increasing chlorinity: $\Delta^{56}Fe_{aq\text{-}eth}$ is greatest at low chlorinity, where $FeCl_2(H_2O)_4^+$ is the dominant species, and smallest at high chlorinity where $FeCl_3(H_2O)_3$ is dominant. The experimental $\Delta^{56}Fe_{aq\text{-}eth}$ ranges from 0.8‰ at $[Cl^-] = 0.5$ M to 0.0‰ at $[Cl^-] = 5.0$ M, a decrease in aqueous–ether fractionation of 0.8‰. This is very close to the theoretically predicted decreases in $\Delta^{56}Fe_{aq\text{-}eth}$, which range from 1.0 to 0.7‰, depending on the ab initio model.

The rate of isotopic exchange and attainment of equilibrium are shown using spiked reversal experiments in conjunction with the two-phase aqueous–ether system. Equilibrium under the experimental conditions is established within 30 min.

The general agreement between theoretical predictions and experimental results points to substantial equilibrium isotopic fractionation among aqueous ferric chloride complexes and a decrease in $^{56}Fe/^{54}Fe$ as the Cl^-/Fe^{3+} ion ratio increases. The effects on isotopic fractionation shown by the modeling of this simple iron–ligand system imply that ligands present in an aqueous environment are potentially important drivers of fractionation, are indicative of possible fractionation effects due to other speciation effects (such as iron–sulfide systems or iron bonding with organic ligands), and must be considered when interpreting iron isotope fractionation in the geological record.

1. INTRODUCTION

Isotopic fractionation among iron-bearing species is found in both geological and biological systems at Earth-

* Corresponding author.
E-mail address: phill@ess.ucla.edu (P.S. Hill).

0016-7037/$ - see front matter © 2009 Elsevier Ltd. All rights reserved.
doi:10.1016/j.gca.2009.01.016

surface temperatures. Large fractionations have been attributed to redox reactions between ferrous and ferric species. Both theoretical studies (Polyakov and Mineev, 2000; Schauble et al., 2001; Anbar et al., 2005; Polyakov et al., 2007; Tang and Liu, 2007; Hill and Schauble, 2008) and experimental studies (e.g., Anbar et al., 2000; Johnson et al., 2002) have demonstrated Fe^{3+}/Fe^{2+} fractionation of at least 2–3‰ at room temperature.

Theoretical studies also indicate that changes in bond partners (i.e., different ligands or coordination numbers) should result in significant isotopic fractionation (Polyakov and Mineev, 2000; Schauble et al., 2001; Polyakov et al., 2007; Hill and Schauble, 2008). The omnipresence of dissolved aqueous species (e.g., chlorides, sulfides, organic ligands, and siderophores) and their potential influence on the solubility, mobility, and availability of iron-bearing species make the isotope geochemistry of aqueous iron complexes an important area of study.

Chloride, a ubiquitous aqueous solute, is of interest as a bonding partner with iron because of its similarity to other likely iron–ligand partners, and its facility in aqueous-phase experiments. For example, S^{2-}, a common partner of iron in both natural and biological systems, has an electronic structure similar to that of Cl^- and can form similar structures with similar $^{56}Fe/^{54}Fe$ trends (Schauble et al., 2001; Polyakov et al., 2007). Ferric chlorides and sulfides/sulfates occur naturally in some highly acidic extreme terrestrial environments if the elemental components are available (e.g., acidic sulfate–chloride lakes or hot springs associated with subaerial volcanic activity (e.g., Delmelle and Bernard, 1994), acidic evaporative basins or lakes (e.g., Bowen et al., 2007), and highly acidic mine tailings such as Spain's Rio Tinto (e.g., Amils et al., 2007) or the Richmond mine, Iron Mountain, California (e.g., Jamieson et al., 2005)).

The formation of Fe^{3+}–Cl^-–H_2O complexes is expected to generate inter-species fractionations nearly as large as the ~3‰ fractionation between Fe^{3+}(aq) and Fe^{2+}(aq) (Schauble et al., 2001; Hill and Schauble, 2008). However, the experimental record is mixed. In low-chlorinity experiments ($[Cl^-] \leqslant 0.1$ mol/L), no isotopic effect has been found (Welch et al., 2003); at higher chloride concentrations (~2 M HCl) in resin/solution partitioning experiments Anbar et al. (2000) found a modest (~0.1‰) fractionation, while Fujii et al. (2006) found fractionations from 1.6 to 0.6‰ between the dominant Fe^{3+}–Cl^- species in an aqueous HCl solution and $FeCl_4^-$ in crown ether at [HCl] = 1.6–3.5 M.

This study integrates experimental studies with theoretical predictions in the aqueous ferric aquo–chloro system to study the effects of solution chemistry and iron–ligand speciation on equilibrium mass-dependent iron isotopic fractionation. We measured the extent of Fe-isotope fractionation among aqueous Fe–Cl complexes relative to a monospecific ether spectator phase, under a range of chloride concentrations (0.5–5.0 mol/L) in low pH solutions, and then compared our results against the theoretical equilibrium mass-dependent isotopic fractionations predicted by several sets of ab initio models developed for these complexes by Hill and Schauble (2008).

These studies demonstrate a potentially significant contribution to iron isotope signatures in natural systems from the non-redox effects of iron–ligand speciation. Further, the techniques used in the present study, viz. separation of a spectator phase using diethyl ether and the use of spiked two-phase equilibrium experiments, can be used to make reversible measurements of both Fe^{3+}/Fe^{2+} fractionation and fractionations associated with small, labile inorganic ligands analogous to biological molecules. These techniques should also be applicable to measurements of isotopic fractionation of other heavy elements in solution.

1.1. Speciation and structures of the ferric chloride complexes

According to several spectroscopic studies (e.g., Lind, 1967; Cotton and Gibson, 1971; Sharma, 1974; Best et al., 1984; Murata and Irish, 1988; Murata et al., 1989), the major complexes in an acidic aqueous solution of ferric chloride are $Fe(H_2O)_6^{3+}$, $Fe(H_2O)_5Cl^{2+}$, $Fe(H_2O)_4Cl_2^+$, $Fe(H_2O)_3Cl_3^0$, and $FeCl_4^-$ (Table 1). Following the convention in Hill and Schauble (2008), we have abbreviated these complexes according to the number of Fe–Cl bonds (i.e., **C0** = $Fe(H_2O)_6^{3+}$, **C1** = $(Fe(H_2O)_5Cl)^{2+}$, etc.). The complexes **C0**, **C1** and **C2** have octahedral geometries, while **C4** is clearly tetrahedral (Magini and Radnai, 1979; Apted et al., 1985). The structure of ferric trichloride **C3** is less certain: it may be either octahedral or trigonal bipyramidal (Lind, 1967; Bjerrum and Lukes, 1986) and was modeled both ways by Hill and Schauble (2008). The octahedral structures of **C2** and **C3** were modeled respectively as *trans* (i.e., with Cl^- on opposite corners of the octahedron) and as *fac* (i.e., with Cl^- ions on the three corners of one face of the octahedron). We used values for **C2** as *trans* and **C3** as *fac* octahedral when calculating our theoretical predications.

There is also evidence for the existence of further complexes such as $FeCl_5(H_2O)^{2-}$ and $FeCl_6^{3-}$ (e.g., Shamir, 1991; Inada and Funahashi, 1999); however, the relative abundances of these complexes in solution are too low to be considered in our experiments. Ferric hydroxide com-

Table 1
Aqueous ferric–chloride complexes.

Ferric Complex	Abbreviation (# Cl atoms)	# Fe–Cl bonds	Charge	Structure
$Fe(H_2O)_6^{3+}$	**C0**	0	+3	Octahedral
$FeCl(H_2O)_5^{2+}$	**C1**	1	+2	Octahedral
$FeCl_2(H_2O)_4^+$	**C2**	2	+1	Octahedral (*trans*)
$FeCl_3(H_2O)_3^0$	**C3**	3	0	Octahedral (*fac*)
$FeCl_4^-$	**C4**	4	−1	Tetrahedral
$Fe(H_2O)_6^{3+}\cdot NO_3^-$		0	+2	Nitrate in outer hydration sphere

plexes are also considered negligible due to the low pH of the solutions (~0); a preliminary report by Liu and Tang (2006) suggests that fractionation of the ferric hydroxides is similar to that of **C0**. Nitric acid (HNO_3) is used in the experiments to control the pH and ionic strength of the solution while allowing for a range of chloride activities. Nitrate is believed to interact weakly with the ferric ion in the outer hydration sphere as $Fe(H_2O)_6^{3+}\cdot NO_3^-$ (Horne et al., 1964; Morris and Sturgess, 1969); preliminary ab initio modeling by Hill and Schauble (2008) indicates that the reduced partition function ratio of $Fe(H_2O)_6^{3+}\cdot NO_3^-$ should be similar to, or slightly smaller than, that of **C0**.

Speciation modeling of the aqueous ferric chloride complexes (this work and others such as Rabinowitch and Stockmayer, 1942; Bjerrum and Lukes, 1986; Bethke, 1996; Lee et al., 2003) indicates that the initial concentration of chloride, the acidity, and the ionic strength of the solution determine the relative concentration of each Fe–Cl complex. As the Cl^-/Fe^{3+} ratio increases, the relative abundances of species with more Fe–Cl bonds increases. The design of our experiments makes use of these changing relative abundances.

1.2. Ether with dissolved $FeCl_4^-$ as spectator phase

We took advantage of the selective solubility of **C4** ($FeCl_4^-$) in organic solvents at low pH to create a separable spectator phase. The use of ether to extract $FeCl_4^-$ from a solution of ferric chloride dissolved in hydrochloric acid is an old technique, developed by J.W. Rothe in the late 1800s (Nachtrieb and Conway, 1948). Because ether and water are immiscible, the ether solution containing the dissolved **C4** forms a separate phase, which rests on top of the aqueous phase.

A monospecific ether phase can easily be equilibrated with an aqueous ferric chloride solution, and quantitatively separated from that solution without disturbing the overall equilibrium of the two-phase solution. This procedure is analogous to the use of CO_2 gas to monitor the oxygen-isotope fractionation behavior of aqueous solutions of varying chemistries (e.g., O'Neil and Truesdell, 1991). The existence of a two-phase system also facilitates reversal experiments, as described below.

Ether extraction of a spectator phase has advantages over precipitation methods (e.g., Johnson et al., 2002) or column elution methods (e.g., Anbar et al., 2000; Mathews et al., 2001). Once the system comes to equilibrium, one need not worry about kinetic effects or further fractionation during the sampling process. Conversely, both precipitation methods and column elution methods involve potential fractionation in order to separate the phases being compared, the effects of which must be subtracted from the measured fractionation.

Early studies showed that the amount of iron extracted by the ether phase (most likely as $FeCl_4\cdot H_3O\cdot nH_2O$) increases as the concentration of iron in the acid solution increases and as the amount of HCl in the solution increases (Dodson et al., 1936; Sandell, 1944; Nachtrieb and Fryxell, 1948). We chose diethyl ether over the less volatile isopropyl ether as a solvent for **C4** because diethyl ether extracts more **C4** from the aqueous phase at low chlorinities than does isopropyl ether (Dodson et al., 1936). Nachtrieb and Conway (1948) noted that the time required for maximum extraction of iron into the ether depends appreciably upon the amount of mixing of the ether and the aqueous solution; more than 98% of the total iron dissolved in the ether was extracted within 20 min after gentle inversions of the solution container. We gave each of our ether–aqueous mixtures a vigorous shake and then let them equilibrate for at least 40 min before proceeding, so that the ether and aqueous phases would have a chance to separate after the initial emulsification.

There is a slight dissolution of hydrochloric acid (i.e., the aqueous phase) into the ether phase upon addition of the ether. Dodson et al. (1936) reported a decrease in the aqueous volume $\leqslant 2\%$ with the addition of an equal amount of ether. For a concentration of 0.0794 M Fe aq, the 2% reduction in volume results in an increased Fe concentration equal to 0.0810 M Fe, not enough to influence the level of accuracy of our experiments. We ran a control experiment with $[Cl^-] = 0.0$ M to ensure that no measurable amount of aqueous iron was extracted into the ether phase without the presence of HCl (see Section 3).

1.3. Ab initio models of equilibrium mass-dependent Fe isotope fractionation in Fe–Cl species

Four different ab initio models of equilibrium mass-dependent Fe isotopic fractionation among the ferric chloride complexes, (from Hill and Schauble, 2008), are used to generate theoretical predictions for the aqueous–ether fractionations resulting from our experiments. The models employ Unrestricted Hartree Fock (UHF) and hybrid Density Functional Theory (DFT), B3LYP (Becke, 1993), methods paired with different basis sets. The UHF model is paired with the 6-31G(d) basis set (Rassolov et al., 1998), and the hybrid DFT models, with basis sets 6-31G(d), 6-311G(d) (Frisch et al., 2004), and Ahlrich's VTZ (Schäfer et al., 1992). 6-31G(d) is a double split-valence basis set; 6-311G(d), a triple split-valence basis set; and Ahlrich's VTZ, a triple zeta basis set. The four models are abbreviated: (1) UHF/6-31G(d); (2) B3LYP/6-31G(d); (3) B3LYP/6-311G(d); and (4) B3LYP/VTZ. The latter model uses Ahlrich's VTZ for Fe and Cl, and basis set 6-31G(d) for O and H. The models are in vacuo, i.e., modeled with only an inner hydration sphere as gas phase molecules.

The reduced partition function ratios (β) of the four models for each complex are listed in Table 2 as 1000 ln β $\beta_{AX} = {}^{56}Fe/{}^{54}Fe$ reduced partition function ratio of AX relative to a dissociated Fe atom X, i.e., iron vapor. 1000 ln β values are in parts permil (‰).

The isotopic fractionations of each complex **Ci** relative to **C4** (denoted as $\alpha_{(Ci-C4)}$) are shown in Fig. 1 where $1000\ \ln\alpha_{(Ci-C4)} = 1000\ \ln\beta_{(Ci)} - 1000\ \ln\beta_{(C4)}$ (i.e., $\alpha_{(Ci-C4)} = \beta_{(Ci)}/\beta_{(C4)}$). The fractionation factor between each complex and **C4** decreases as the number of Fe–Cl bonds increases (Table 3). The ranges of fractionation between **C0** and **C4** predicted by the models are ~1.5–2.5‰.

Table 2
Equilibrium Fe isotopic fractionation (1000 ln β) for the Fe–Cl complexes at 293.15 K (20 °C) from four of the ab initio models of Hill and Schauble (2008).

Complex	UHF/6-31G(d)	B3LYP/631G(d)	B3LYP/6311G(d)	B3LYP/VTZ
C0	9.73	8.93	9.41	9.59
C1	9.12	8.04	8.54	8.57
C2	8.73	7.61	8.1	8.13
C3[a]	7.74	7.05	7.13	7.13
C4	8.25	7.46	7.17	7.14

[a] **C3** modeled as $FeCl_3(H_2O)_3$ (*fac* octahedral structure).

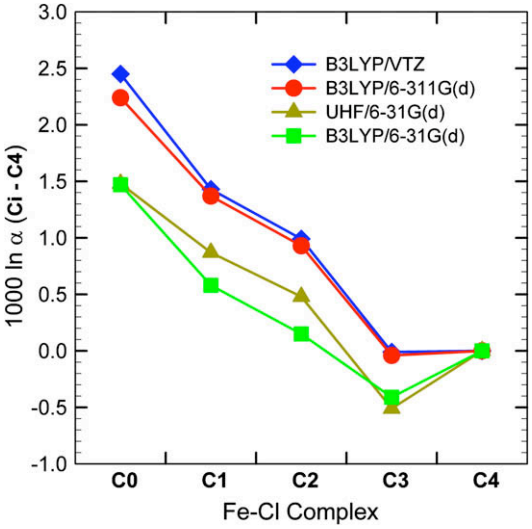

Fig. 1. Predicted Fe isotopic fractionation of ferric chloride complexes (**Ci**) relative to **C4** expressed as 1000 ln α where 1000 ln α (**Ci–C4**) = 1000 ln β (**Ci**)–1000 ln β (**C4**) (Hill and Schauble, 2008). (Compare with Tables 2 and 3.)

Table 3
Predicted Fractionation of **C0** Relative to **C4** expressed as 1000 ln α where $1000 \ln \alpha_{(C0-C4)} = 1000 \ln \beta_{(C0)} - 1000 \ln \beta_{(C4)}$ (Hill and Schauble, 2008). (See Fig. 1.)

	UHF/6-31G(d)	B3LYP/6-31G(d)	B3LYP/6-311G(d)	B3LYP/VTZ
1000 ln α (**C0–C4**)	1.48	1.47	2.24	2.45

2. METHODS

2.1. Fractionation experiment procedures

2.1.1. Aqueous phase

Series of aqueous ferric chloride solutions (20 ml each) were created from stock solutions of crystalline ferric nitrate $Fe(NO_3)_3 \cdot 9(H_2O)$, ([Fe] = 0.0794 mol/L). The ferric nitrate crystals were ultra pure (>99.9%) in order to avoid contamination by Cr in the MC-ICPMS (See Section 2.1.4.). In each series the chlorinity was varied from 0.5 to 5.0 M by the addition of HCl. Total acidity was held constant ([H+] = 5 mol/L), as well as the initial ionic strength (~5 – see Section 3.2 on speciation), by adding appropriate amounts of HNO_3. All measurements were made with an Eppendorf™ auto-pipette. The solutions were gently shaken and then allowed to rest for 10 min in a separation funnel.

Fig. 2. Separation of ether and aqueous phases in a ferric chloride solution. The ether phase is on the top.

2.1.2. Ether phase

An equal volume of immiscible diethyl ether was added to the aqueous solution. The ether–aqueous mixture was briskly shaken, and then allowed to rest for at least 40 min. The ether almost immediately formed a separate, less dense, liquid phase on top of the aqueous phase. During this time, a portion of $FeCl_4^-$ passed from the aqueous phase into the ether phase, turning the ether phase a pale–yellow color. A sharp boundary between the aqueous and ether phases was visible almost immediately (Fig. 2). No second ether phase was seen; the formation of a second phase, mentioned by Dodson et al. (1936), appears to require chlorinity ⩾7 M. Some $FeCl_4^-$ is also expected to remain in the aqueous phase.

When the ether–aqueous mixture is shaken, there is a tendency for a very small amount of the mixture to escape from the top of the separation funnel, due to the increased vapor pressure of the ether. Loss of solution was avoided by gentle release and then reinsertion of the funnel cap. Volumetric ether measurements were made with a 25 ml graduated glass cylinder.

2.1.3. Separation of phases

After the designated equilibrium time had elapsed in each experiment, separate aliquots of the ether (1 ml) and aqueous (0.25 ml) phases were removed immediately by disposable pipette from the top of the funnel and through the stopcock at the bottom of the funnel, respectively, to Savillex™ beakers for isotopic analysis. One milliliter of 1 M HCl was added to each ether sample to ensure dissolution of all iron as the ether evaporated. The samples were dehydrated on a hot plate (100 °C for aqueous samples; 50 °C for ether samples) to remove any remaining HCl, and then

rehydrated with dilute nitric acid. Further dilutions were made with 2% nitric acid as necessary to match the concentration of the Fe isotope standard used for mass spectrometry.

A few milliliters of aqueous solution were allowed to run through the stopcock before samples were gathered for analysis. The aqueous sample was then gathered in a glass beaker, from which measurements were made with an auto-pipette.

The volatility of ether causes problems with an auto-pipette. Therefore, measurements of the ether solution were taken with a disposable pipette with gradations at 0.25 ml. We found that the ether in the disposable pipette has less tendency to shoot out prematurely if the pipette is held vertically.

2.1.4. Isotopic measurements

The Fe isotope ratios $^{56}Fe/^{54}Fe$ and $^{57}Fe/^{54}Fe$ of both the aqueous phase and the ether phase for each sample were measured on the UCLA Thermo Finnegan Neptune MC-ICPMS (Multiple Collector Inductively Coupled Plasma Mass Spectrometer). The instrument has a fixed array of nine Faraday collectors with $10^{11}\ \Omega$ amplifiers. The mass spectrometer was operated at a mass resolving power of ~12,000 (M/dm) to eliminate ArO^+, $ArOH^+$, and ArN^+ mass interferences at cardinal masses 56, 57 and 54, respectively (e.g., Weyer and Schwieters, 2003). Solutions were inspected for $^{52}Cr^+$ to monitor possible interference from $^{54}Cr^+$. In all cases, Cr was found to be below detection levels. Potential instrumental mass bias due to inter-element matrix effects was not an issue since samples consisted of pure Fe. Samples were run in dry plasma using a desolvating nebulizer (Cetac Aridus) at ~1 ppm Fe in ~2% HNO_3.

Iron isotope ratios were corrected for instrumental fractionation using standard-sample-standard bracketing. Isotope ratios are reported as $\delta^{56}Fe$ and $\delta^{57}Fe$ values relative to a standard:

$$\delta^{i}Fe = 10^{3}\left(\frac{(^{i}Fe/^{54}Fe)_{Sample}}{(^{i}Fe/^{54}Fe)_{Std}} - 1\right) \quad (1)$$

where i represents either 56 or 57, *Std* represents the in-house standard, and *Sample* signifies the sample. In this study all Fe isotope ratios are reported relative to the working standard Spex-1; the isotopic composition of this standard is related to the IRMM14 iron standard by the experimentally determined $\delta^{56}Fe(IRMM14) = 0.99979\ (\delta^{56}Fe(Spex\text{-}1)) - 0.20845$.

Iron isotope fractionation between aqueous Fe and ethereal $FeCl_4^-$ is expressed as $\delta^{56}Fe_{(aq\text{-}eth)} = \delta^{56}Fe_{aq}$ (total Fe in aqueous phase) $- \delta^{56}Fe_{eth}$ ($FeCl_4^-$ in ether phase). Values for $\Delta^{56}Fe_{(aq\text{-}eth)}$ were determined for aqueous–ether pairs of each molarity of Cl^-.

2.1.5. Fe concentration measurements

The concentration of total iron in both the ether and aqueous phases for each sample was measured with a GENESYS 20 spectrophotometer using the ferrozine method (Stookey, 1970; Vollier et al., 2000). Ferrozine interacts with ferrous iron to create a purple–hued complex; the intensity of the color depends on the concentration of Fe^{2+}. The reducing agent hydroxylamine hydrochloride was added to the samples to reduce all ferric species. Ten times the required amounts of reducing agent and of ferrozine were added to the sample to ensure that all ferric iron reacted.

Maximum absorbance for iron occurs between pH values of 4 and 9 at a wavelength of 562 nm (Stookey, 1970). We added an acetic acid–ammonium hydroxide buffer of pH ~5.7 to the samples to ensure the correct range of pH values. Reducer, ferrozine, and buffer were premixed in a 1:2:4 ratio and then added to the samples to facilitate the measurement process.

Since the absorbency of samples drifts slightly over time, each sample with added ferrozine, reducer, and buffer was allowed to rest a uniform ten minutes before measurement in the spectrophotometer.

The molar absorptivity constant for our spectrophotometer, determined empirically by measurement of aliquots of known standards, is 26107 ± 144[1], in reasonable agreement with measurements by other workers (e.g., 27,000 molar absorbtivity, Stookey, 1970). Samples were diluted to [Fe] = ~40 μM (absorbancy = ~1) via 2 to 3 separate dilution steps, using an Eppendorf™ auto-pipette. The first dilution(s) were with deionized water; the last with the reducer–ferrozine–buffer mixture. All aqueous samples were diluted and measured independently at least three times.

Measuring the iron concentration in the ether phase posed potential problems because the ether evaporates rapidly, leaving behind an unknown volume of solution. To avoid this problem, we removed 3 ml of ether solution from the separation funnel to a 10 ml graduated glass cylinder with a disposable pipette. We immediately added 1 ml of 1 M HCl to the cylinder and then set the cylinder aside for a few days, lightly covered with Parafilm™, until all the ether had evaporated. Deionized water was added to the remaining liquid to return the total volume to 3 ml. The resultant iron solution concentration, with ether removed and with a known dilution factor, was then measured with the spectrophotometer as described above. Each sample was diluted and measured three times independently. However, measurements of ethereal iron have larger errors than aqueous iron measurements due to the additional measurement error from the use of both a disposable pipette and a graduated cylinder in the first steps of the measurement process. All three sets of separate dilution measurements for the ethereal iron sample will include the same error resulting from the graduated cylinder and disposable pipette. Therefore, all three ethereal measurements will have the same component of this bias in their resultant measurement errors.

Two other measuring techniques for the ether phase were also tried: (1) A known amount of ether phase was added immediately to a premeasured amount of reducer–buffer–ferrozine mix and covered with parafilm for 10 min before going to the spectrophotometer. (2) A known amount of ether phase with added 1 M HCl was put into

[1] Standard error one sigma; a relative standard error of ~0.5%.

a Petri dish and partially covered with the Petri dish lid to hasten evaporation of the ether (due to a larger surface area). Then an additional measured amount of 1 M HCl was added to the dish and gently swirled to pick up any remnants of Fe. However, measurements from these two methods were not as reproducible as the graduated cylinder method described above.

2.2. Reversal experiments

Reversal experiments demonstrate equilibrium by running the same reaction in opposite directions (forward and reverse), thereby bracketing the equilibrium point from two different paths. In the forward experiment, the direction of iron transport is from the aqueous phase into the ether phase as some $FeCl_4^-(aq)$ dissolves into the ether phase

$$\sum_{n=0}^{3} FeCl_n(H_2O)_{6-n}{}^{3-n}(aq) + FeCl_4{}^-(aq) \Rightarrow \sum_{n=0}^{3} FeCl_n(H_2O)_{6-n}{}^{3-n}(aq) + FeCl_4{}^-(aq) + FeCl_4{}^-(eth) \quad (2)$$

This creates an isotopic fractionation between the aqueous and ether phases, the magnitude of which is dependent upon the chlorinity of the solution.

In the reversal experiment, the direction of iron transport is from the ether phase into the aqueous phase. Ether containing spiked **C4** (i.e., $^{54}FeCl_4^-$) is added to the ether of a forward, isotopically normal experiment, which has already achieved equilibrium. This forces isotopic transport of spiked **C4** from the ether phase into the aqueous phase, where speciation and isotopic exchange with the aqueous iron occur. Further exchange will take place between the ether and the aqueous phases until an isotopic equilibrium is reached.

$$^{54}FeCl_4^-(eth) \Rightarrow {}^{54}FeCl_4{}^-(aq) \Rightarrow \sum_{n=0}^{3} {}^{54}FeCl_n(H_2O)_{6-n}{}^{3-n}(aq) + {}^{54}FeCl_4{}^-(aq) \quad (3)$$

$$^{54}FeCl_4{}^-(aq) + \sum_{n=0}^{3} {}^{56}FeCl_n(H_2O)_{6-n}{}^{3-n}(aq) \Longleftrightarrow {}^{56}FeCl_4{}^-(aq) + \sum_{n=0}^{3} {}^{54}FeCl_n(H_2O)_{6-n}{}^{3-n}(aq) \quad (4)$$

$$^{54}FeCl_4^-(eth) + {}^{56}FeCl_4^-(aq) \Longleftrightarrow {}^{56}FeCl_4^-(eth) + {}^{54}FeCl_4^-(aq) \quad (5)$$

If equilibrium is attained in these experiments, the resultant fractionation between the aqueous and ether phases should be the same as the interphase fractionation of a forward experiment of the same chlorinity, acidity and nitrate concentration.

The ether with spiked **C4** for the reversal experiment was prepared via a forward experiment prepared with aqueous ^{54}Fe spike. Both the spiked and normal solutions had $[Cl^-] = 1.0$ M. Once each mixture equilibrated, half the ether (10 ml) from the spiked experiment (containing excessive $^{54}FeCl_4^-$) was added to the ether of the normal - isotope forward experiment, creating the reversal experiment. Thus, the reversal experiment began at time $t = 0$ with 20 ml aqueous phase and 30 ml ether phase. We measured the rate and progress of the reversal experiment toward equilibrium by removing small aliquots from both the ether and aqueous phases after 20, 30 and 40 min (without disturbing the mixtures) and measuring the aqueous–ether isotopic fractionation at each time step.

In order to quantify progress towards equilibrium, we used the three-isotope exchange method to bracket equilibrium (Matsuhisa et al., 1978; Mathews et al., 1983; Shahar et al., 2008). This method is based on the exponential relationship between the equilibrium mass-dependent fractionation factors $\alpha_{i-j}^{b/a}$ and $\alpha_{i-j}^{c/a}$ between phases i and j for three different isotopes a, b, and c of a given element (Matsuhisa et al., 1978; Young et al., 2002). In this case,

$$\alpha^{56/54} = (\alpha^{57/54})^{\gamma} \quad (6)$$

$$\gamma = (1/m_{54} - 1/m_{56})/(1/m_{54} - 1/m_{57}) \quad (7)$$

$$\text{and} \qquad 10^3 \ln(\alpha^{56/54}) = \gamma 10^3 \ln(\alpha^{57/54}) \quad (8)$$

where atomic masses m_i are: $m_{54} = 53.93961$, $m_{56} = 55.93494$, and $m_{57} = 56.93540$ amu (Baum et al., 2002). Using these values the exponent $\gamma = 0.678$. In δ notation the above equilibrium relationship between the three isotopes becomes

$$\delta^{56}Fe = (1000 + \delta^{56}Fe_{ref})\,[(1000 + \delta^{57}Fe) / (1000 + \delta^{57}Fe_{ref})]^{\gamma} - 1000 \quad (9)$$

where *ref* refers to any point on the above fractionation line. In three-Fe-isotope space ($\delta^{56}Fe$ vs. $\delta^{57}Fe$) Eq. (9) defines a slightly curved, primary (terrestrial) mass fractionation line, along which naturally occurring, iron-bearing terrestrial samples lie (Matsuhisa et al., 1978; Young et al., 2002).

At the start of the reversal experiment, when the spiked ether is added to the ether of the unspiked forward experiment, the resulting ether mixture lies off the terrestrial mass fractionation line (TFL) due to excess ^{54}Fe (Fig. 3). Isotopic exchange between the spiked ether phase and the unspiked aqueous phase will establish equilibrium along a secondary fractionation line (SFL), parallel to, but below the first (Fig. 3). The position in three-isotope space of the new SFL will pass through the bulk composition of the mixture, signified as $\delta^{56}Fe_0$ and $\delta^{57}Fe_0$ (Mathews et al., 1983). The location of the bulk composition in 3-isotope space is defined by isotopic mass balance such that

$$(^{56}Fe/^{54}Fe)_0 = (^{56}Fe/^{54})_{aq} * (f) * ([Fe_{aq}]/[Fe_0]) + (^{56}Fe/^{54}Fe)_{eth} * (1-f) * ([Fe_{eth}]/[Fe_0]) \quad (10)$$

$$\text{and } [Fe_0] = f * [Fe_{aq}] + (1-f) * [Fe_{eth}] \quad (11)$$

Note $(^{56}Fe/^{54}Fe)_0$, $(^{56}Fe/^{54})_{aq}$, and $(^{56}Fe/^{54}Fe)_{eth}$ are the isotopic ratios of the bulk composition the aqueous phase, and the ether phase respectively; f is the fractional volume of the aqueous phase to the total volume; and $[Fe_{aq}]$, $[Fe_{eth}]$, and $[Fe_0]$ are the concentrations of Fe in the aqueous phase, the ether phase, and the entire solution in moles/liter (Faure, 2005).

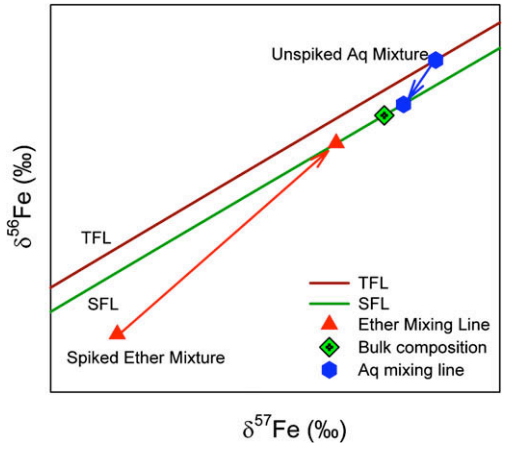

Fig. 3. Schematic diagram of progression of a reversal experiment toward equilibrium in three-isotope space. At time = 0, the aqueous phase (top right blue hexagon) sits on the terrestrial mass fractionation line (TFL) while the ether phase, with excess $^{54}FeCl_4^-$, rests below the TFL (red triangle in lower left corner). As the mixture equilibrates isotopically, both phases move toward equilibrium on the secondary mass fractionation line (SFL) (lower line), each along its own mixing line. The ether phase moves up along the lower (red) line while the aqueous phase moves down along the upper (blue) line in the direction of the arrows. The SFL must pass through the bulk composition of the two phases, shown by the green diamond. Equilibrium is achieved when both phases lie on the SFL. The distance between the two phases once on the SFL (in terms of $\delta^{56}Fe$) is $\Delta^{56}Fe_{aq-eth}$. (For interpretation of the references to colours in the figure legend, the reader is referred to the web version of this paper.)

An analogous relationship holds for ^{57}Fe. $\delta^{56}Fe_o$ and $\delta^{57}Fe_o$ are then calculated from Eq. (1).

As isotopic exchange progresses toward equilibrium, the ether phase will move up a mixing line toward a position on the SFL while the aqueous phase will travel down its own mixing line toward its position on the same mass fractionation line (Fig. 3). Equilibrium is reached when both phases arrive at the new equilibrium mass fractionation line (i.e., the SFL). The distance between the two phases (in terms of $\delta^{56}Fe$) on the SFL should ideally be equal to the $\Delta^{56}Fe_{aq-eth}$ of the forward experiment.

Equilibrium is thus demonstrated in two ways: (1) Fe isotopic composition in both the ether and the aqueous phases of the reversal experiment moves to the same mass fractionation line, and 2) the $\Delta^{56}Fe_{(aq-eth)}$ values of both the forward and the reversal experiments are the same within analytical uncertainties.

Fe concentrations of each phase of the reversal experiment were measured at 40 min (in order to minimize disruption of the reversal experiment) and are used in calculating the bulk isotopic composition of the mixture.

3. RESULTS

3.1. Dissolution of $FeCl_4^-$ into the ether phase

The percentage of total iron extracted from the aqueous phase by dissolution into the diethyl ether phase increases as the chlorinity of the solution increases, changing the ether from a pale yellow to a deep amber color. In our experiments, in which both pH and ionic strength are held roughly constant (~0 and ~5, respectively), the ethereal iron climbs from 0.0% at 0.0 M Cl^- to >95% at 5.0 M (Table 4 and Fig. 4).

When acidity, ionic strength, and chlorinity increase together, as a function of increasing concentrations of HCl, the amount of initial iron dissolved into diethyl ether increases more slowly (Dodson et al., 1936). Apparently dissolution of $FeCl_4^-$ increases as both more H^+ and Cl^- are made available because the iron is most likely extracted as stoichiometric $HFeCl_4^-$ (i.e., $FeCl_4{\cdot}H_3O{\cdot}nH_2O$ see section 1.2). Dodson et al.'s ethereal iron concentrations are shown in Fig. 4 for comparison.

Mass balance calculations of aqueous and ether iron concentration measurements are on average within 8% of the total initial iron (comparable with the total uncertainty obtained by propagation of measurement error – see Table 4). This is similar to mass balance molarity measurements by Nachtrieb and Conway (1948). Measurement errors of

Table 4
Division of total iron between aqueous and ether phases for different chlorinities. Each concentration was measured independently at least three times. Reported errors are standard error 1σ and are the original measurement errors propagated through 2–4 separate dilution steps. Units are mol/liter. Total Fe is the calculated concentration of the original iron solution before the addition of ether. Fe aq and Fe eth are measured quantities. Fe aq errors result from measurement with an auto-pipette while Fe eth errors contain measurements errors from an auto-pipette, a disposable pipette, and a 10 ml graduated cylinder (see Section 2.1.5). (See Fig. 4.)

Cl^-	Total Fe	Fe aq	Fe eth	Fe aq + Fe eth	Fe eth/(Fe aq + Fe eth)	Fe aq/(Fe aq + Fe eth)
0.0	0.0794	0.079 ± 0.0003	0.000 ± 0.0000	0.079 ± 0.0003	0.0000	1.0000
0.5	0.0794	0.078 ± 0.0003	0.003 ± 0.0001	0.080 ± 0.0003	0.0359	0.9641
0.5	0.0794	0.073 ± 0.0007	0.001 ± 0.0000	0.074 ± 0.0007	0.0129	0.9871
1	0.0794	0.085 ± 0.0001	0.005 ± 0.0001	0.090 ± 0.0001	0.0546	0.9454
1	0.0794	0.068 ± 0.0011	0.008 ± 0.0002	0.075 ± 0.0011	0.1032	0.8968
1.5	0.0794	0.057 ± 0.0000	0.029 ± 0.0008	0.086 ± 0.0008	0.3386	0.6614
1.75	0.0794	0.042 ± 0.0001	0.035 ± 0.0008	0.076 ± 0.0008	0.4524	0.5476
3	0.0794	0.018 ± 0.0000	0.074 ± 0.0018	0.092 ± 0.0018	0.8017	0.1983
3	0.0794	0.019 ± 0.0000	0.066 ± 0.0016	0.085 ± 0.0016	0.7742	0.2258
3	0.0794	0.019 ± 0.0002	0.065 ± 0.0039	0.084 ± 0.0039	0.7748	0.2252
4	0.0794	0.012 ± 0.0001	0.073 ± 0.0019	0.085 ± 0.0019	0.8616	0.1384
5	0.0794	0.004 ± 0.0002	0.086 ± 0.0023	0.090 ± 0.0023	0.9513	0.0487
5	0.0794	0.004 ± 0.0001	0.079 ± 0.0042	0.083 ± 0.0042	0.9555	0.0445

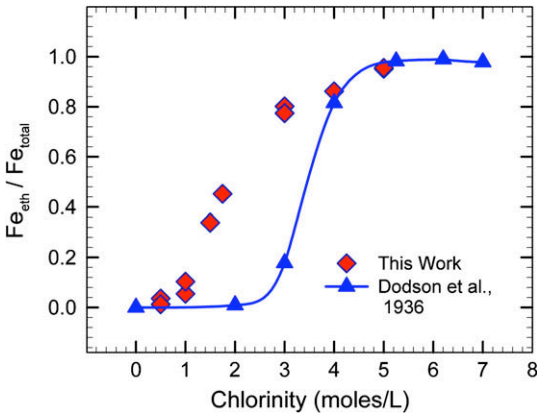

Fig. 4. Percentage of total initial iron extracted into ether phase for various chlorinities. The amount of ethereal iron from this work is compared to experiments from Dodson et al. (1936) in which both $[H^+]$ and $[Cl^-]$ were increased together (as [HCl]); in our experiments $[H^+] = 5$ M for all $[Cl^-]$. The greater dissolution of Fe into the ether phase at lower chlorinities in our experiments shows that $[H^+]$ is a limiting factor since the ethereal iron is probably dissolved as stoichiometric $HFeCl_4$ (see Section 1.2). (See Table 4.)

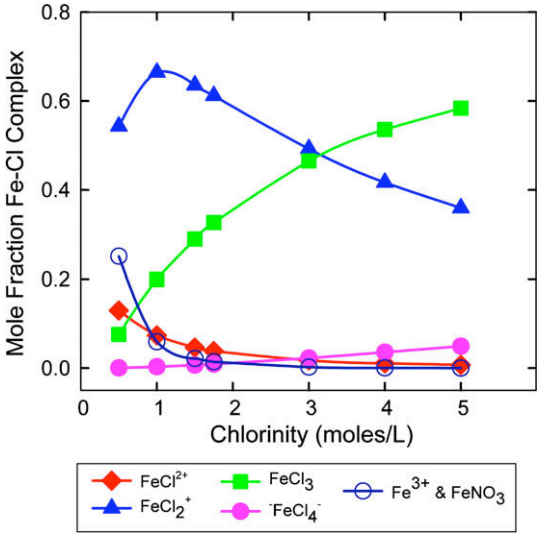

Fig. 5. Mole fractions of the individual Fe–Cl complexes, at varying $[Cl^-]$, relative to the total amount of iron remaining in the aqueous phase after dissolution of some $FeCl_4^-$ into the ether phase. (See Table 5.)

ethereal iron concentration in general are larger than those of aqueous iron due to the volatility of the ether and to differences in the measurement process (see Section 2.1.5 for further error discussion). Measurements may also be slightly affected by minute change in volume due to the dissolution of some HCl (i.e., the aqueous phase) into the ether phase (see Section 1.2).

3.2. Speciation of FeCl complexes with varying chlorinities

The relative abundances of the aqueous ferric chloride complexes depend on the amount of available chloride, the acidity, and the ionic strength of the aqueous solution. As the chlorinity to iron ratio increases, Fe–Cl species with more Fe^{3+}–Cl^- bonds become more plentiful (Fig. 5 and Table 5). According to our speciation models, with pH ~0 and ionic strength ~5, **C2** is the most abundant complex between 0.5 and 3 M chlorinity, while **C3** is most abundant from ~3.2 to 5 M chlorinities. **C4** abundances are initially low but increase continuously with rising chlorinity. **C0** and $Fe(H_2O)_6^{3+}{\cdot}NO_3^-$ and, to a lesser extent, **C1**, are important at $[Cl^-] = .5$–1 M, but decease rapidly at higher $[Cl^-]$.

Our models for the ferric chloride complexes at each chloride concentration were calculated using the FeCl association equilibrium constants for **C1**, **C2**, **C3** and **C4** (30, 4.5, 0.15 and 0.0078 respectively) from Bjerrum and Lukes (1986), the $FeNO_3^{2+}$ association equilibrium constant (10) from Delany and Lundeen (1990), and the activity models for HCl and HNO_3 from Bromley (1973). Calculations were iterated to determine final ionic strength and species concentrations. At each chlorinity, the amount of aqueous iron (i.e., the amount of iron left in the aqueous phase after dissolution of some iron into the ether phase – see Table 4) was used as the total aqueous iron concentration. Since $FeCl_4^-$ is dissolved into the ether phase as stoichiometric $HFeCl_4$ ($FeCl_4{\cdot}H_3O^+{\cdot}nH_2O$ see Section 1.2), the initial aqueous chloride concentration was decreased by four times the amount of ethereal iron while the initial aqueous H^+ concentration was decreased by the amount of ethereal iron. (For example, at $[Cl^-] = 3$ M and $[Fe_{total}] = 0.0794$ M, $[Fe_{aq}] = 0.017$ M so the amounts of Fe^{3+}, Cl^- and H^+ sequestered from the aqueous to the ether phase are $[Fe_{eth}] = 0.06$ M, $[Cl_{eth}^-] = 0.024$ M and $[H_{eth}^+] = 0.06$M. Thus, $[Cl_{aq}^-] = 2.976$ M and $[H_{aq}^+] = 4.94$ M). These small changes in aqueous concentrations

Table 5
Calculated mole fractions of each Fe–Cl complex, for varying chlorinities, relative to the total moles of aqueous iron, after equilibration with the ether phase. Ave. Fe aq is calculated from the average percentage of Fe aq (Table 4, column 7) based on an initial total calculated Fe = .0794 M. (See Fig. 5.)

Ave Fe aq (M)	Cl^-	$Fe(H_2O)_6^{3+}$	$FeCl(H_2O)_5^{2+}$	$FeCl_2(H_2O)_4^+$	$FeCl_3(H_2O)_3$	$FeCl_4^-$	$Fe(H_2O)_6{\cdot}NO_3^{2+}$
0.077	0.5	0.005	0.130	0.543	0.076	0.001	0.246
0.073	1.0	0.001	0.074	0.664	0.199	0.003	0.058
0.053	1.5	0.001	0.047	0.636	0.289	0.007	0.021
0.043	1.75	0.000	0.038	0.612	0.327	0.009	0.014
0.017	3.0	0.000	0.017	0.492	0.465	0.023	0.002
0.011	4.0	0.000	0.011	0.417	0.536	0.036	0.001
0.004	5.0	0.000	0.007	0.359	0.584	0.049	0.000

of Fe, Cl and H did not have a noticeable impact on speciation.

Some speciation models of ferric chloride complexes vs. chlorinity are shown in which chlorinity is increased by adding increasing amounts of HCl (e.g., Roe et al., 2003; Fujii et al., 2006). In these models, in contrast to our model, pH decreases and the ionic strength increases in the aqueous solution as chlorinity increases, resulting in a slightly different distribution of ferric chloride complex abundances (discussed further in Section 4.5).

The presence of nitrate ions in the aqueous solution at low chlorinities influences the speciation of iron by causing formation of $Fe(H_2O)_6^{3+}{\cdot}NO_3^-$ in addition to $Fe(H_2O)_6^{3+}$. In our experiments the NO_3^- ion is most abundant at the very lowest chlorinities, since the amount of nitric acid necessary to keep the pH constant decreases as more HCl is added.

Complexation of the nitrate ion with some of the iron sequesters part of the iron that might otherwise have gone into iron chloride species, but this apparently has no significant effect on the relative abundances of the non-nitrate complexes nor the dissolution of Fe into the ether.

3.3. Experimental fractionation between aqueous and ether phases with increasing chlorinity

The measured fractionation between the aqueous and ether phases, defined as $\Delta^{56}Fe_{(aq-eth)} = \delta^{56}Fe$ (total Fe remaining in aqueous phase)$-\delta^{56}Fe$ ($FeCl_4^-$ in ether phase), shows a clear downward trend with the increasing chlorinity (Table 6 and Fig. 6). At $[Cl^-] = 0.5$ M, $\Delta^{56}Fe_{aq-eth} = 0.8‰$; at 5.0 M, 0.0‰. The $\delta^{56}Fe$ and $\delta^{57}Fe$ experimental values plot along the terrestrial mass fractionation line, a demonstration of mass dependent fractionation and a lack of Cr interference (Section 2.1.4) (Fig. 7).

Isotopic Fe mass balance calculations on aqueous–ether pairs were within ±0.05 ‰ of the initial ferric nitrate stock solution.

3.4. Predicted $\Delta^{56}Fe_{aq\text{-}eth}$ from the ab initio fractionation models

Predictions of $\Delta^{56}Fe_{aq-eth}$ using the four ab initio models were calculated as

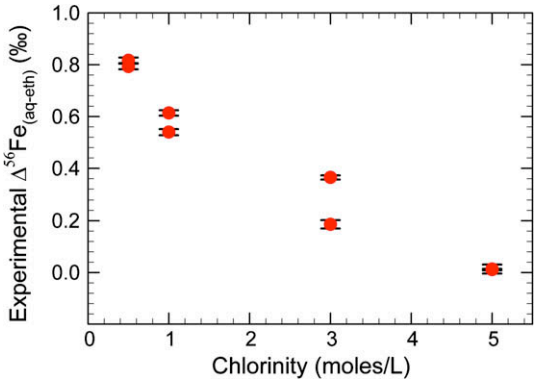

Fig. 6. Experimental data for $\Delta^{56}Fe_{aq-eth} = \delta^{56}Fe$ (total Fe remaining in aqueous phase)$-\delta^{56}Fe$ ($FeCl_4^-$ in ether phase) (‰). (pH ~0, T = 20 °C). (See Table 6.)

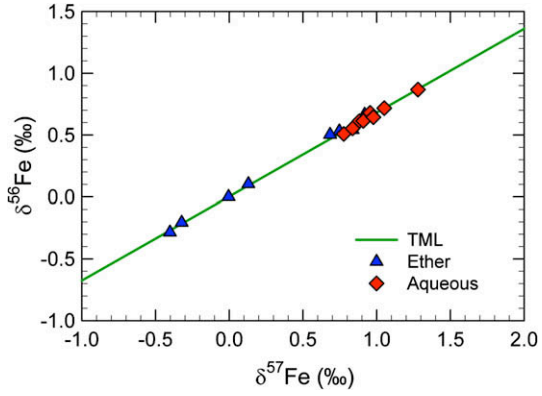

Fig. 7. Experimental values of $\delta^{56}Fe$ (‰) and $\delta^{57}Fe$ (‰) pairs from $\Delta^{56}Fe_{aq-eth}$ (‰) plotted along the terrestrial mass fractionation line. Error bars represent 1-sigma standard error. The error bars are smaller than the plotted symbols on the graph. (See Table 6.)

$$\Delta^{56}Fe_{aq-eth} = \sum_i (1000\ \ln \beta_{FeCl_i})(X_{i\,aq}) - 1000\ \ln \beta_{FeCl_4^-\,ether} \quad (12)$$

where X_i is the fraction of Fe in complex i (relative to total Fe in the aqueous solution) and β_{FeCl_i} is the reduced partition function ratio for the i^{th} FeCl complex. This assumes there is no fractionation between $\mathbf{C4}_{aq}$ and $\mathbf{C4}_{eth}$ when **C4**

Table 6
Measured fractionation (in ‰) between aqueous and ether phases, defined as $\Delta^{56}Fe_{(aq-eth)} = \delta^{56}Fe$ (total Fe remaining in aqueous phase)–$\delta^{56}Fe$ ($FeCl_4^-$ in ether phase), versus chlorinity. $\delta^{56}Fe$ and $\delta^{57}Fe$ for both ether and aqueous phases are shown, expressed relative to the inhouse standard Fe Spex-1 (see Section 2.1.4). Standard errors are for 1 sigma. The ether rest time is the time in minutes between the addition of ether to the aqueous solution and the removal of aqueous and ether samples for isotopic measurement. (See Fig. 6.)

Exp't	Cl	$\Delta^{56}Fe_{(aq-eth)}$	Aq $\delta^{56}Fe$	Ether $\delta^{56}Fe$	Aq $\delta^{57}Fe$	Ether $\delta^{57}Fe$	Ether rest time (min)
FN30	0.5	0.817 ± 0.011	0.611 ± 0.013	−0.206 ± 0.007	0.882 ± 0.020	−0.323 ± 0.023	41
FN23	0.5	0.793 ± 0.011	0.509 ± 0.011	−0.284 ± 0.016	0.777 ± 0.017	−0.402 ± 0.023	45
FN31	1	0.614 ± 0.010	0.614 ± 0.003	0.000 ± 0.011	0.909 ± 0.017	−0.005 ± 0.024	45
FN20	1	0.540 ± 0.012	0.644 ± 0.016	0.104 ± 0.010	0.978 ± 0.015	0.130 ± 0.016	42
FM32	3	0.186 ± 0.016	0.717 ± 0.004	0.531 ± 0.017	1.051 ± 0.010	0.747 ± 0.013	41
FN21	3	0.365 ± 0.008	0.868 ± 0.011	0.503 ± 0.008	1.280 ± 0.017	0.684 ± 0.008	42
FN33	5	0.014 ± 0.017	0.679 ± 0.018	0.666 ± 0.006	0.956 ± 0.015	0.918 ± 0.016	45
FN22	5	0.011 ± 0.003	0.553 ± 0.011	0.542 ± 0.011	0.837 ± 0.015	0.836 ± 0.011	45

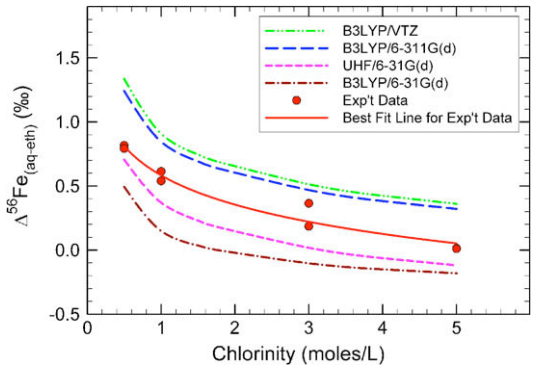

Fig. 8. Comparison of ab initio model predictions and experimental data for $\Delta^{56}Fe_{aq-eth}$ vs. chlorinity. The solid (red) line is a logarithmic best fit to the experimental data; best fit equations for experimental data and model predictions are listed in Table 9. (See Tables 6 and 7.) (For interpretation of the references to colours in the figure legend, the reader is referred to the web version of this paper.)

Table 7
Predictions of $\Delta^{56}Fe_{aq-eth}$ (‰) for each chlorinity, calculated from the fractional concentrations of each Fe–Cl complex and the corresponding ab initio 1000 ln β factors. The predicted differences in $\Delta^{56}Fe_{aq-eth}$ (‰) for $[Cl^-] = 0.5$ and 5.0 M are shown in the last row. (See Fig. 8.)

Cl^- (M)	UHF/ 6-31G(d)	B3LYP/ 6-31G(d)	B3LYP/ 6-311G(d)	B3LYP/ VTZ
0.5	0.71	0.49	1.24	1.34
1.0	0.37	0.15	0.84	0.91
1.5	0.23	0.04	0.69	0.75
1.8	0.18	0.00	0.64	0.69
3.0	0.02	−0.10	0.47	0.51
4.0	−0.06	−0.15	0.38	0.42
5.0	−0.12	−0.18	0.32	0.36
$\Delta^{56}Fe_{aq-eth}$ (Cl = 0.5 M)−Δ^{56} Fe_{aq-eth} (Cl = 5.0 M)	0.82	0.68	0.92	0.98

dissolves into the ether. All four ab initio models and the experimental results display a similar decrease in the aqueous–ether fractionation with increasing chlorinity (Fig. 8, Tables 6 and 7). Eq. (12) is derived from the following relationships.

$$\Delta^{56}Fe_{aq-eth} = \delta^{56}Fe_{AX} - \delta^{56}Fe_{BX} \quad (13)$$

$$1000\ ln\,\alpha_{(AX-BX)} \sim \delta^{56}Fe_{AX} - \delta^{56}Fe_{BX} \quad (14)$$

$$\alpha_{(AX-BX)} = \frac{\beta_{AX-X}}{\beta_{BX-X}} \quad (15)$$

$$1000\ \ln\ \alpha_{(AX-BX)} = 1000\ \ln\beta_{AX-X} - 1000\ \ln\beta_{BX-X} \quad (16)$$

Preliminary calculations indicate that the reduced partition function ratio for $Fe(H_2O)_6^{3+}\cdot NO_3^-$ is similar to that of **C0**; hence, $Fe(H_2O)_6^{3+}\cdot NO_3^-$ was treated as **C0** (see Hill and Schauble, 2008).

3.5. Reversal experiments

The attainment of equilibrium within thirty minutes is demonstrated in two ways. First, at thirty minutes both the forward and the reversal experiments achieved similar values of $\Delta^{56}Fe_{aq-eth}$: 0.828 ± 0.0415‰ (1 sigma std err) and 0.783 ± 0.0249‰, respectively (Table 8 and Fig. 9). Second, both the aqueous and ether phases of the reversal experiment have arrived at the same equilibrium mass fractionation line (SFL – see section 2.2) in three-isotope space in time t, where $20 < t \leqslant 30$ min. On a plot of $\delta^{57}Fe$ vs. $\delta^{56}Fe$, at the start of the reversal experiment ($t = 0$), the unspiked aqueous phase and the spiked ether phase are on different mass fractionation lines. At $t = 20$ min, both phases have moved much closer; the ether phase has reached 99.8%[2] of its equilibrium $\delta^{56}Fe_{eth}$, $\Delta^{56}Fe_{aq-eth}$ at 20 min is at 97.4%[2] of its equilibrium value, while the aqueous phase has achieved 71%[2] of its final $\delta^{56}Fe$ at 20 min (see Section 4.4). At 30 min, both phases are on the same SFL.

The location of the bulk composition of the equilibrated mixture in 3-isotope space, as calculated from the measurements of Fe concentrations and delta values at $t = 40$ min (Table 8), also lies on the SFL as it should (see Section 2.2). ($\delta^{57}Fe$, $\delta^{56}Fe$ (bulk composition)) = (−3.50 ± .02‰, −3.70 ± .02‰, std err 1 sigma) (Fig. 9).

4. DISCUSSION

4.1. Fractionation among the Fe–Cl complexes

The most significant feature of both the theoretical and the experimental $\Delta^{56}Fe_{aq-eth}$ data is the prominent smooth decrease in aqueous–ether isotopic fractionation with rising chlorinity (Fig. 8). Experiments show a decrease in fractionation from 0.8‰ at 0.5 M Cl to 0.0‰ for 5.0 M Cl. The theoretical models predict a decrease of 0.7 to 1.0 ‰, depending on the details of the ab initio method (Table 7).

The close agreement of the experimental results with theoretical predictions strongly supports the presence of notable fractionation resulting from speciation and/or complexing in the ferric iron–chloride–water system. This is significant for two reasons: (1) it is of similar order of magnitude to Fe^{3+}/Fe^{2+} fractionation; and (2) it implies that ligands present in an aqueous environment are potentially important drivers of fractionation, and must also be considered when interpreting iron fractionation in geological records.

The reduction in aqueous–ether phase fractionation with increasing chlorinity is most simply explained by the changes in aqueous solution chemistry. As chlorinity rises, species with higher Cl/Fe ratios become more abundant, thus decreasing the overall isotopic fractionation of the aqueous phase relative to **C4** ($FeCl_4^-$) in the ether phase (see Figs. 1 and 5). This trend toward reduction of $^{56}Fe/^{54}Fe$ of the aqueous solution due to solution chemistry should also be apparent in fractionation between the solution and any associated minerals (see Hill and Schauble, 2008).

A comparison of the theoretical models with the experimental data shows that they all have the same quasi-loga-

[2] We define the % equilibrium value of $X = 100\ (X_{@20min} - X_{@0min})/(X_{@30min} - X_{@0min})$ where X is $\delta^{56}Fe_{eth}$, $\delta^{56}Fe_{aq}$, or $\Delta^{56}Fe_{aq-eth}$.

Table 8
Results of spiked reversal experiment. (A) $\delta^{56}Fe$, $\delta^{57}Fe$, and $\Delta^{56}Fe_{aq-eth}$ of the unspiked iron solution before the ether containing spiked $FeCl_4^-$ is added. (B) $\delta^{56}Fe$, $\delta^{57}Fe$, and $\Delta^{56}Fe_{aq-eth}$ of the mixed solution at 20, 30 and 40 min after the spiked ether is added to the ether of the unspiked solution. (C) Fe concentration measurements of aqueous and ether phases at 40 min. (Uncertainties are standard error one sigma.) $\delta^{56}Fe$ and $\delta^{57}Fe$ are expressed relative to the inhouse standard Fe Spex-1 (see Section 2.1.3). (See Fig. 9.)

A	Forward experiment (unspiked)	
	$\delta^{56}Fe$	$\delta^{57}Fe$
Aqueous phase	0.615 ± .0234	0.905 ± .0436
Ether phase	−0.213 ± .0342	−0.336 ± .0300
$\Delta^{56}Fe_{aq-eth}$	0.828 ± 0.0415	
Spiked ether in paired exp't	−148.177 ± .0441	−148.165 ± .0191

B	Reversal experiment (after adding spiked ether)							
Mixture	0 min		20 min		30 min		40 min	
	$\delta^{56}Fe$	$\delta^{57}Fe$	$\delta^{56}Fe$	$\delta^{57}Fe$	$\delta^{56}Fe$	$\delta^{57}Fe$	$\delta^{56}Fe$	$\delta^{57}Fe$
Aqueous Phase	0.615 ± .0234	0.905 ± .0436	−2.369 ± .0308	−2.108 ± .0646	−3.57 ± .0215	−3.301 ± .0349	−3.648 ± .0161	−3.421 ± .0423
Mixed Ether Phase	−49.534[a]	−49.6124	−4.450 ± .0419	−4.571 ± .0631	−4.355 ± .0126	−4.467 ± .0196	−4.403 ± .0239	−4.477 ± .0505
$\Delta^{56}Fe_{aq-eth}$			2.082 ± 0.0520		0.783 ± 0.0249		0.755 ± 0.0288	

C	Fe Concentrations at 40 min		
	[Fe] (mol/L)	Volume (ml)	% total Fe
Aqueous phase	.0711 ± 0.0027	20	~92.8
Mixed ether phase	.0037 ± 2.4∗10^{-5}	30	7.2

[a] Calculated (based on 20 ml unspiked ether + 10 ml spiked ether); could not be measured directly since combined ether was not yet thoroughly mixed at $t = 0$.

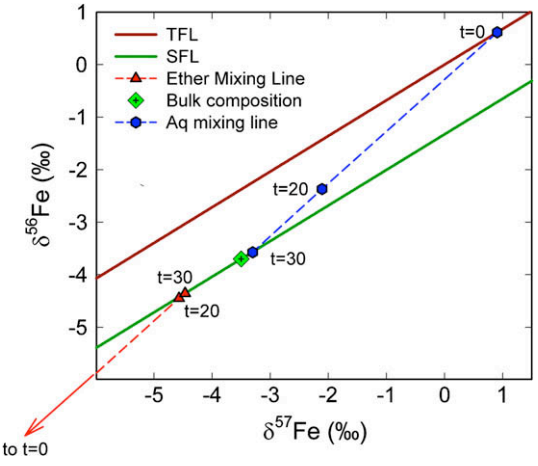

Fig. 9. Progress of aqueous and ether phases toward equilibrium in the reversal experiment in 3-isotope space. The aqueous phase starts on the TFL at time $t = 0$ min, progresses along its mixing line toward the SFL ($t = 20$), and has reached the SFL at $t = 30$. At the same time the ether phase progresses along its mixing line toward the SFL, is almost at the SFL at $t = 20$, and has reached the SFL at $t = 30$. The bulk composition of the mixture is closer to the aqueous phase because that phase contains most of the iron. The $\delta^{56}Fe$ distance between the ether and aqueous phases on the SFL is $\Delta^{56}Fe_{aq-eth}$ (=0.78‰). (See Table 8.)

rithmic downward trend with increasing chlorinity. Table 9 shows the very similar, best fit logarithmic formulas and Pearson correlation R^2 for each model and the experimental data. Hill and Schauble (2008) remark that the two "best" models are B3LYP/VTZ and B3LYP/6-311G(d), since they are calculated with the largest basis sets. However, surprisingly, our experimental data fit in between the "better" and the "worse" models.

To some extent this may be attributed to errors inherent in the model parameter approximations and to measurement errors in the experimental data.

All four theoretical models match the shape of the experimental curve quite well for chlorinities from 1 to 5 M but overpredict fractionation for $[Cl^-] = 0.5$ M. Two possible explanations for this misfit could be: (1) the theoretical predictions of $\Delta^{56}Fe_{aq\text{-}eth}$ use 1000 ln β from **C0** for both $Fe(H_2O)_6^{3+}\cdot NO_3^-$ and **C0** on the assumption that 1000 ln β is quite similar for both species (see Section 3.4). Because $Fe(H_2O)_6^{3+}\cdot NO_3^-$ is in greatest abundance at very low chlorinity (where more HNO_3 is present in order to control the pH and ionic strength), the use of 1000 ln β from **C0** for $Fe(H_2O)_6^{3+}\cdot NO_3^-$ has the largest effect at the lowest chlorinity. The lower value of the experimental $\Delta^{56}Fe_{aq-eth}$ at low chlorinity may suggest that 1000 ln β for $Fe(H_2O)_6^{3+}\cdot NO_3^-$ is somewhat smaller than 1000 ln β for

Table 9
Best fit quasi-logarithmic equations for the experimental $\Delta^{56}Fe_{aq-eth}$ data and for the predicted $\Delta^{56}Fe_{aq-eth}$ from each of the four theoretical models. The variable x represents the chlorinity of the aqueous solution while y represents $\Delta^{56}Fe_{aq-eth}$ (See Fig. 8).

Model	Best fit log equation	R^2 (Pearson correlation)
Experimental data	$y = -0.3298 \ln(x) + 0.5836$	$R^2 = 0.9615$
UHF/6-31G(d)	$y = -0.3488 \ln(x) + 0.4065$	$R^2 = 0.9829$
B3LYP/6-31G(d)	$y = -0.2765 \ln(x) + 0.2074$	$R^2 = 0.9301$
B3LYP/6-311G(d)	$y = -0.3853 \ln(x) + 0.8959$	$R^2 = 0.9747$
B3LYP/VTZ	$y = -0.4074 \ln(x) + 0.9655$	$R^2 = 0.9711$

C0. 2) Another possibility is that the equilibrium constant for $FeNO_3^{2+}$ is too large, resulting in an overestimate of the amount of ferric nitrate (see Section 3.2).

The effects of fractionation shown by the modeling of the simple Fe–Cl complexing system are suggestive of possible fractionation effects in other iron-ligand systems. Cl^- can be considered as a crude analogue for other potential natural ligands such as S^{2-}, organics, etc., with which iron in solution might bond.

4.2. Potential sources of error

Fractionation among aqueous complexes was simulated in vacuo by the ab initio models, on the assumption that this is a reasonable first-order approximation. Preliminary modeling with additional water molecules in an outer hydration sphere indicates that this assumption may introduce some error, especially for **C0**, though the overall trends appear to be robust. A fuller discussion of model limitations and comparison of model vibrational frequencies and bond lengths with experimental data can be found in Hill and Schauble (2008).

Assumptions about the amount of $Fe(H_2O)_6^{3+}{\cdot}NO_3^-$ present in the aqueous solution at very low chlorinities and the use of the **C0** 1000 $\ln\beta$ for $Fe(H_2O)_6^{3+}{\cdot}NO_3^-$ may introduce some error. However, since the nitrate ion is in the second hydration sphere of the ferric ion, these effects are probably quite small. A true comparison of any effects due to nitrate must be made with models of the ferric chloride complexes with second hydration spheres (see Hill and Schauble, 2008).

Variations in the experimental results and in calculations based upon these results are subject to measurement errors. Such errors in measurement of Fe concentration are larger for ethereal iron than for aqueous iron due to the volatility of ether and the measurement procedures (see Sections 1.2 and 3.1). These errors are propagated through other calculations such as predictions for $\Delta^{56}Fe_{aq-eth}$.

4.3. Extraction of the spectator phase using ether

The use of diethyl ether to extract $FeCl_4^-$ as a monospecific spectator phase has implications for a wide range of other isotope fractionation experiments. The $FeCl_4^-$–ether phase was used to monitor the isotopic fractionation behavior of the aqueous solution under varying chemistries (e.g., different chlorinities). Since the aqueous phase reaches equilibrium with the spectator phase rapidly ($\sim 10^3$ s), aliquots of either phase can easily be removed for measurement without disturbing the fractionation of the system components. The existence of two phases in the system also facilitates reversal experiments.

4.4. Equilibrium reversal experiments

Equilibrium in the reversal experiment was attained within 30 min after initially mixing the ether and aqueous phases vigorously. At twenty minutes, $\Delta^{56}Fe_{aq-eth}$ was at 97.4% of its equilibrium value (as defined in Section 3.5, footnote 2) (Fig. 9). In bulk iron partitioning experiments with similar chemistry, Nachtrieb and Conway (1948) also attained 98% equilibrium within 20 min (see Section 1.2).

However, at 20 min $\delta^{56}Fe_{aq}$ was at only 71% of its final value. Most likely the ether and aqueous phases had equilibrated at their interface, which is a very broad surface in the middle of the separation funnel, but the aqueous phase needed longer than 20 min to mix internally, since its volume in the lower end of the separation funnel is deep and narrow (Fig. 2). The reversal experiment has a larger ether phase (30 ml compared to 20 ml) and a much greater difference between the values of δ^{56}Fe aq at times $t = 0$ and 30 min ($\sim 4‰$ compared to $<1‰$) than the normal forward experiment, yet $\Delta^{56}Fe_{aq-eth}$ of the reversal experiment was at 97.4% equilibrium at $t = 20$ minutes. So it is reasonable to assume that $\Delta^{56}Fe_{aq-eth}$ at 20 min for the normal forward experiment will be even closer to the equilibrium value. All our experiments had an ether rest time (Table 6) of at least 40 min.

4.5. Comparison of our theoretical predictions with experimental data from Fujii et al. (2006)

Fujii et al. (2006) measured $\Delta^{56}Fe_{aq-eth}$ from an aqueous Fe–Cl solution in which the concentration of HCl was varied from 1.6 to 3.5 M (resulting in an increase in acidity and ionic strength with chlorinity). Crown ether was used to extract $FeCl_4^-$ as a spectator phase. To compare their results with ours, we used the same speciation parameters (using equilibrium constants from Bjerrum and Lukes (1986) and the HCl activity model from Bromley (1973)) (see Section 3.2) to calculate the relative abundances of the ferric chloride complexes **C0**–**C4** (Table 10 and Fig. 10) in their experiments, and then used the Hill and Schauble (2008) ab initio models to predict $\Delta^{56}Fe_{aq-eth}$ for their experiment, (assuming no fractionation due to the dissolution of **C4** into the crown ether) (Table 11 and Fig. 11) (see Section 3.4). The amount of aqueous iron at each chlorinity was calculated from the distribution ratio D ($=Fe_{eth}/Fe_{aq}$) from the Fujii et al. (2006) data. The amounts of aqueous chloride and hydrogen were adjusted to account for the chloride and hydrogen dissolved into the crown ether along with $FeCl_4^-$ as stoichiometric $HFeCl_4^-(FeCl_4{\cdot}H_3O^+{\cdot}nH_2O$; compare with Section 3.2) although this had no significant effect on the relative fractions of the respective Fe–Cl aqueous species. The results of our speciation calculations for their experimental setup

Table 10
Mole fraction concentrations of aqueous Fe–Cl complexes calculated for Fujii et al. (2006) experiments, relative to total amount of Fe remaining in the aqueous phase after dissolution of some $FeCl_4^-$ into the crown ether. (See Fig. 10).

HCl	Fractional amount of total aq Fe of each complex					
	Fe aq (M)	$Fe(H_2O)_6^{3+}$	$FeCl(H_2O)_5^{2+}$	$FeCl_2(H_2O)_4^{+}$	$FeCl_3(H_2O)_3$	$FeCl_4^-$
1.6	0.0143	0.003	0.111	0.726	0.158	0.002
2.0	0.0097	0.001	0.079	0.706	0.210	0.003
2.1	0.0083	0.001	0.073	0.699	0.224	0.004
2.7	0.0024	0.000	0.045	0.640	0.307	0.008
3.0	0.0012	0.000	0.035	0.605	0.350	0.011
3.5	0.0004	0.000	0.023	0.540	0.420	0.017

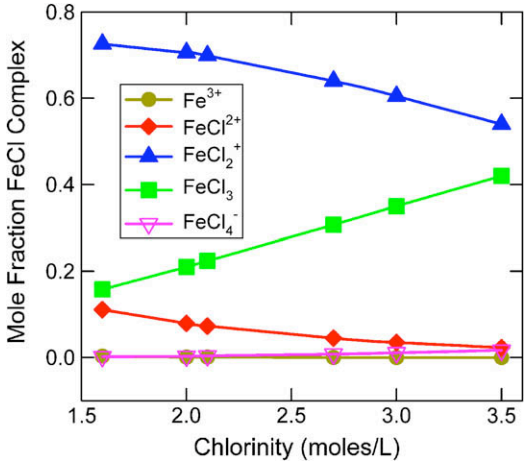

Fig. 10. Fractional concentrations of the individual Fe–Cl complexes for increasing [HCl] (see Table 10) for data from Fujii et al. (2006) relative to the total amount of iron remaining in the aqueous phase after dissolution of some $FeCl_4^-$ into the crown ether. Amounts of chloride and hydrogen in the aqueous phase have also been adjusted to account for the H and Cl dissolved into the crown ether. (See text for discussion.)

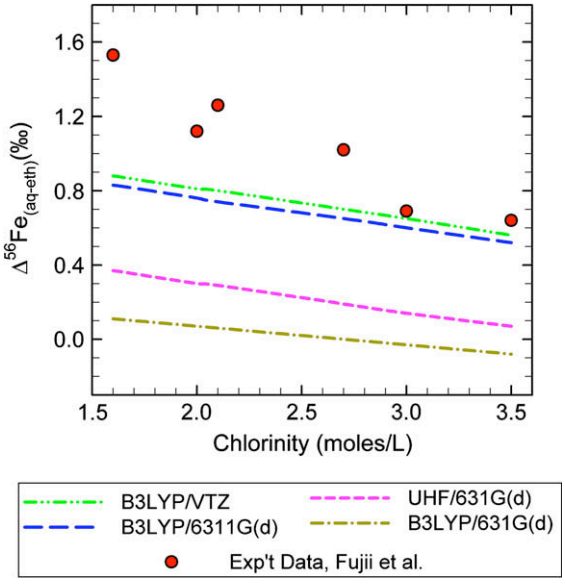

Fig. 11. Comparison of ab initio model predictions with experimental results of $\Delta^{56}Fe_{aq-eth}$ (‰) in Fe–Cl solutions in which [HCl] is varied. Experimental data from Fujii et al. (2006). (See Table 11.)

Table 11
Predicted values of $\Delta^{56}Fe_{aq-eth}$ (‰) for Fujii et al. (2006) experiments using ab initio models of Hill and Schauble (2008). (See Fig. 11.)

[HCl]	Predicted $\Delta^{56}Fe_{aq-eth}$ from ab initio models				Exp't $\Delta^{56}Fe_{aq-eth}$ (Fujii et al., 2006)
	UHF/631G(d)	B3LYP/631G(d)	B3LYP/6311G(d)	B3LYP/VTZ	
1.6	0.37	0.11	0.83	0.88	1.530
2.0	0.30	0.07	0.76	0.81	1.120
2.1	0.29	0.06	0.74	0.80	1.260
2.7	0.19	0.00	0.65	0.70	1.020
3.0	0.14	−0.03	0.60	0.65	0.690
3.5	0.07	−0.08	0.52	0.56	0.640

(i.e., simultaneous increases in both H^+ and Cl^-) are very similar to their speciation results.

The two "best" ab initio models (B3LYP/6-311G(d) and B3LYP/VTZ) match the Fujii et al. (2006) experimental results fairly well for [HCl] ⩾ 3 M, but underpredict fractionation at 1.6 < [HCl] < 3 M (Table 11 and Fig. 11). As expected, there is a downward trend of $\Delta^{56}Fe_{aq-eth}$ as [Cl] increases; however, the linear rate of decrease in fractionation is greater when both the acidity and the chlorinity increase together (Fujii et al. data) (slope = −0.42‰/M with $R^2 = .89$) than when acidity and ionic strength are held constant (our data) (slope = -0.16‰/M with $R^2 = .94$) (Figs. 11 and 8 respectively). The mismatch between our theoretical predictions and the Fujii et al. (2006) data at smaller chlorinities (<3 M) is puzzling since the theoretical predictions match fairly well with our data for [Cl^-] ⩾ 1 M (Fig. 8).

One possibility is that the Hill and Schauble (2008) β value for **C2** is too small. A comparison of the relative mole fractions of **C2** and **C3** in the range of 1.5 M ⩽ [Cl^-] ⩽ 3 M between our data (with constant pH and ionic strength) and the Fujii et al. data (with increasing pH and ionic strength) (Tables 5 and 10 respectively) shows that **C2** is the domi-

Table 12
Comparison of relative concentrations of **C2** to **C3** for [Cl^-] at 1.5–1.6 M and 3 M for Fujii et al. (2006) data and data from this work. Data are taken from speciation models shown in Tables 5 and 10.

[Cl^-]	**C2/C3** (Fujii et al., 2006)	**C2/C3** (this work)
1.5 or 1.6	4.8	2.4
3	1.7	1.1

nant species within this range for both datasets, but that the Fujii et al. data is almost twice as sensitive to β for **C2** than is our data (due to its greater relative abundance), especially for [Cl^-] ~ 1.5 M (Table 12).

5. CONCLUSIONS

We performed experimental studies of equilibrium isotopic fractionation among the aqueous ferric chloride complexes and then compared the results with predictions from the four sets of ab initio models for each complex developed by Hill and Schauble (2008). Experiments consisted of low pH, constant ionic strength solutions of aqueous ferric chloride with chlorinity ranging from 0.5 to 5.0 M. A spectator phase, created by the dissolution of $FeCl_4^-$ into a separate monospecific diethyl ether phase, was used to monitor changes in fractionation in the aqueous phase as chlorinities increased. Key to these experiments is the increase in the relative abundance of the Fe–Cl complexes with more Fe–Cl bonds and the resulting decrease in relative fractionation among these aqueous complexes as the chlorinity increases.

All the ab initio models predict a decrease in isotopic fractionation of the ferric chloride complexes relative to $FeCl_4^-$ as the Cl^-/Fe^{3+} ratio increases. This is demonstrated in both the experimental results and the theoretical predictions by the decrease in fractionation between the aqueous system and the ether phase with increasing chlorinity.

The good agreement between our experimental data and the model predictions suggests a potential equilibrium fractionation of 1.5–2.5‰ between **C0** and **C4**, comparable to that of fractionation due to redox reactions, implying that ligands present in the chemical environment of any aqueous iron reactions, as well as the redox state, are potentially important drivers of fractionation and must be taken into account when attempting to interpret the isotopic fractionation of iron-bearing species in geological and biological systems.

The rate and attainment of solution isotopic equilibrium was demonstrated by the use of the two-phase system in combination with a spiked reversal experiment. This is an important and straightforward technique to deal with the troublesome problem of demonstrating equilibrium in an aqueous system.

The modeling of the ferric chloride system as an example of a simple iron-ligand system is also suggestive of possible fractionation effects due to other speciation effects, such as iron–sulfide systems or iron bonding with organic ligands.

The creation of a spectator phase by dissolution of a single species into ether may well be applicable to a wider range of isotope fractionation experiments. The use of ether to investigate iron speciation and its isotopic consequences has advantages over precipitation methods or column elution methods in that once the system comes to equilibrium, removal of part of the ether phase does not disturb the equilibrium of the aqueous phase (and vice versa). This experimental technique can easily be extended to make reversible measurements of Fe^{3+}/Fe^{2+} fractionation and fractionations associated with other inorganic and organic Fe ligand bonds.

ACKNOWLEDGMENTS

We wish to thank Craig Manning for helpful comments on speciation modeling. We also appreciate the thoughtful comments from V.B. Polyakov, associate editor Thomas Chacko, and an anonymous reviewer. This research was funded in part by National Science Foundation, Grant No. EAR 0643286 to EAS, the NASA Astrobiology Institute, and the UCLA IGPP Center for Astrobiology.

REFERENCES

Amils R., González-Toril E., Fernández-Remolar D., Gómez F., Aguilera A., Rodríguez N., Malki M., García-Moyano G., Fairén A. G., de la Fuente V. and Sanz J. L. (2007) Extreme environments as Mars terrestrial analogs: the Rio Tinto case. *Planet. Space Sci.* **55**, 370–381.

Anbar A. D., Jarzecki A. A. and Spiro T. G. (2005) Theoretical investigation of iron isotope fractionation between $Fe(H_2O)_6^{3+}$ and $Fe(H_2O)_6^{2+}$: implications for iron stable isotope geochemistry. *Geochim. et Cosmochim. Acta* **69**, 825–837.

Anbar A. D., Roe J. E., Barling J. and Nealson K. H. (2000) Nonbiological fractionation of iron isotopes. *Science* **288**, 126–128.

Apted M. J., Waychunas G. A. and Brown G. E. (1985) Structure and specification of iron complexes in aqueous solutions determined by X-ray absorption spectroscopy. *Geochim. et Cosmochim. Acta* **49**, 2081–2089.

Baum E. M., Knox H. D. and Miller T. R. (2002) *Nuclides and isotopes chart of the nuclides*, 16th ed. KAPL, Inc., Niskayuna, NY.

Becke A. D. (1993) Density-functional thermochemistry: III. The role of exact exchange. *J. Chem. Phys.* **98**, 5648–5652.

Best S. P., Beattie J. K. and Armstrong R. S. (1984) Vibrational spectroscopic studies of trivalent hexa-aqua-cations: single-crystal raman spectra between 275 and 1200 cm^{-1} of the Caesium Alums of Titanium, Vanadium, Chromium, Iron, Gallium and Indium. *J. Chem. Soc., Dalton Trans.* **12**, 2611–2624.

Bethke C. M. (1996) *Geochemical reaction modeling concepts and applications*. New York, Oxford University Press.

Bjerrum J. and Lukes I. (1986) The Iron(III)–Chloride system. A study of the stability constants and of the distribution of the tetrachloro Species between organic solvents and aqueous chloride solutions. *Acta Chem. Scand. Series A—Phys. Inorg. Chem* **15**, 31–40.

Bromley L. A. (1973) Thermodynamic properties of strong electrolytes in aqueous solution. *AIChE J.* **19**, 313–320.

Bowen B. B., Benison K. C., Oboh-Ikuenobe F. and Mormile M. (2007) Hematite concretions from modern acid saline lake sediments as geochemical and astrobiological tombs. *LPS*. Seventh Int. Conf. Mars. #3175 (abstr.).

Cotton S. A. and Gibson J. F. (1971) Spectroscopic studies of some Aquo-complexes of Iron (III) and Indium (III). *Inorg. Phys. Theor., J. Chem. Soc. (A)* **11**, 1693–1696.

Delany J.M. and Lundeen S. R. (1990) The LLNL thermochemical database. Lawrence Livermore National Laboratory Report UCRL-21658, p. 150.

Delmelle P. and Bernard A. (1994) Geochemistry, mineralogy, and chemical modeling of the acid crater lake of Kawah-Ijen Volcano, Indonesia. *Geochim. Cosmochim. Acta* **58**, 2445–2460.

Dodson R. W., Forney G. J. and Swift E. H. (1936) The extraction of ferric chloride from hydrochloric acid solutions by isopropyl ether. *J. Am. Chem. Soc* **58**, 2573–2577.

Faure G. (2005) *Isotopes Principles and Applications*, Third ed. Wiley, New York, 897 p.

Frisch M. J., Trucks G. W., Schlegel H. B., Scuseria G. E., Robb M. A., Cheeseman J. R., Montgomery Jr., J. A., Vreven T., Kudin K. N., Burant J. C., Millam J. M., Iyengar S. S., Tomasi J., Barone V., Mennucci B., Cossi M., Scalmani G., Rega N., Petersson G. A., Nakatsuji H., Hada M., Ehara M., Toyota K., Fukuda R., Hasegawa J., Ishida M., Nakajima T., Honda Y., Kitao O., Nakai H., Klene M., Li X., Knox J. E., Hratchian H. P., Cross J. B., Adamo C., Jaramillo J., Gomperts R., Stratmann R. E., Yazyev O., Austin A. J., Cammi R., Pomelli C., Ochterski J. W., Ayala P. Y., Morokuma K., Voth G. A., Salvador P., Dannenberg J. J., Zakrzewski V. G., Dapprich S., Daniels A. D., Strain M. C., Farkas O., Malick D. K., Rabuck A. D., Raghavachari K., Foresman J. B., Ortiz J. V., Cui Q., Baboul A. G., Clifford S., Cioslowski J., Stefanov B. B., Liu G., Liashenko A., Piskorz P., Komaromi I., Martin R. L., Fox D. J., Keith T., Al-Laham M. A., Peng C. Y., Nanayakkara A., Challacombe M., Gill P. M. W., Johnson B., Chen W., Wong M. W., Gonzalez C. and Pople J. A. (2004) Gaussian 03, (Revision C.02). Gaussian, Inc., Wallingford CT.

Fujii T., Moynier F., Telouk P. and Albarède F. (2006) Isotope fractionation of Iron(III) in chemical exchange reactions using solvent extraction with crown ether. *J. Phys. Chem. A* **110**, 11108–11112.

Hill P. S. and Schauble E. A. (2008) Modeling the Effects of Bond Environment on Equilibrium Iron Isotope Fractionation in Ferric Aquo–Chloro Complexes. *Geochim. Cosmochim. Acta* **72**, 1939–1958.

Horne R. A., Myers B. R. and Frysinger G. R. (1964) The effect of pressure on the dissociation of Iron(III) monochloride complex ion in aqueous solution. *Inorg. Chem.* **3**, 452–454.

Inada Y. and Funahashi S. (1999) Equilibrium and structural study of chloro complexes of iron(III) in acidic aqueous solution by means of x-ray absorption spectroscopy. *Z. Naturforsch. B Chem. Sci.* **54**, 1517–1523.

Jamieson H. E., Robinson C., Alpers C. N., Nordstrom D. K., Poustovetov A. and Lowers H. A. (2005) The composition of coexisting jarosite-group minerals and water from the Richmond mine, Iron Mountain, California. *Can. Mineral.* **43**, 1225–1242.

Johnson C. M., Skulan J. L., Beard B. L., Sun H., Nealson K. H. and Braterman P. S. (2002) Isotopic fractionation between Fe(III) and Fe(II) in aqueous solutions. *Earth Planet. Sci. Lett.* **195**, 141–153.

Lee M. S., Ahn J. G. and Oh Y. J. (2003) Chemical model of the $FeCl_3$–HCl–H_2O solutions at 25C. *Mater. Trans.* **44**, 957–961.

Lind M. D. (1967) Crystal structure of ferric chloride hexahydrate. *J. Chem. Phys.* **47**, 990–993.

Liu Y. and Tang M. (2006) Iron isotopic fractionations between species in solution – From ab initio quantum chemistry calculations. *Geochim. et Cosmochim. Acta Supplement* **70**, 367 (abstr.).

Magini M. and Radnai T. (1979) X-ray diffraction study of ferric chloride solutions and hydrated melt. Analysis of the iron (III) – chloride complexes formation. *J. Chem. Phys* **71**, 4255–4262.

Mathews A., Goldsmith J. R. and Clayton R. N. (1983) On the mechanisms and kinetics of oxygen isotope exchange in quartz and feldspars at elevated temperatures and pressures. *GSA Bull.* **94**, 396–412.

Mathews A., Zhu X. K. and O'Nions K. (2001) Kinetic iron stable isotope fractionation between iron (-II) and (-III) complexes in solution. *Earth Planet. Sci. Lett.* **192**, 81–92.

Matsuhisa Y., Goldsmith J. R. and Clayton R. N. (1978) Mechanisms of hydrothermal crystallization of quartz at 250 C and 15 kbar. *Geochim. Cosmochim. Acta* **42**, 173–182.

Morris D. F. C. and Sturgess P. J. (1969) Formation of an Iron(III) nitrate complex. *Electrochim. Acta* **14**, 629–631.

Murata K. and Irish D. E. (1988) Raman studies of the hydrated melt of $FeCl_3{*}6H_2O$. *Geochim. et Cosmochim. Acta* **44A**, 739–743.

Murata K., Irish D. E. and Toogood G. E. (1989) Vibrational spectral studies of solutions at elevated temperatures and pressures. II. A Raman spectral study of aqueous iron(III) chloride solutions between 25 and 300 C. *Can. J. Chem* **67**, 517–524.

Nachtrieb N. H. and Conway J. G. (1948) The extraction of ferric chloride by isopropyl ether I. *J. Am. Chem. Soc.* **70**(11), 3547–3552.

Nachtrieb N. H. and Fryxell R. E. (1948) The extraction of ferric chloride by isopropyl ether II. *J. Am. Chem. Soc.* **70**(11), 3552–3557.

O'Neil J.R. and Truesdell A.H. (1991) Oxygen isotope fractionation studies of solute water interactions. In *Stable Isotope Geochemistry: A Tribute To Samuel Epstein*(eds. Taylor, O'Neil, and Kaplan). Geochemical Society Special Pub. No. 3.

Polyakov V. B., Clayton R. N., Horita J. and Mineev S. D. (2007) Equilibrium iron isotope fractionation factors of minerals: Reevaluation from the data of nuclear ineleastic resonant X-ray scattering and Mössbauer spectroscopy. *Geochim. et Cosmochim. Acta* **71**, 3833–3846.

Polyakov V. B. and Mineev S. D. (2000) The use of Mössbauer spectroscopy in stable isotope geochemistry. *Geochim. et Cosmochim. Acta* **64**, 849–865.

Rabinowitch E. and Stockmayer W. H. (1942) Association of ferric ions with chloride, bromide and hydroxyl ions (A spectroscopic study). *J. Am. Chem. Soc* **64**, 335–347.

Roe J. E., Anbar A. D. and Barling J. (2003) Nonbiological fractionation of Fe isotopes: evidence of an equilibrium isotope effect. *Chem. Geol.* **195**, 69–85.

Rassolov V. A., Pople J. A., Ratner M. A. and Windus T. L. (1998) 6-31G(d) basis set for atoms K through Zn. *J. Chem. Phys.* **109**, 1223–1229.

Sandell E. B. (1944) *Colorimetric Determination Of Traces Of Metals*. Interscience, Publishers, New York.

Schäfer A., Horn H. and Ahlrichs R. (1992) Fully optimized contracted Gaussian-basis sets for atoms Li to Kr. *J. Chem. Phys.* **97**, 2571–2577.

Schauble E. A., Rossman G. R. and Taylor, Jr., H. P. (2001) Theoretical estimates of equilibrium Fe-isotope fractionations from vibrational spectroscopy. *Geochim. et Cosmochim. Acta* **65**, 2487–2497.

Shahar A., Manning C. E. and Young E. D. (2008) Equilibrium high-temperature Fe isotope fractionation between fayalite and magnetite: an experimental calibration. *Earth Planet. Sci. Lett.* **268**(3-4), 330–338.

Shamir J. (1991) Raman and infrared spectra of the FeCl63– Anion: comparison of MCl4 and MCl6 vibrational frequencies. *J. Raman Spectrosc.* **22**, 97–99.

Sharma S. K. (1974) Raman study of ferric chloride hexahydrate and ferric chloride hexadeutrate in crystalline, Molten and Glassy States. *J. Non-Cryst. Solids* **15**, 83–95.

Stookey L. L. (1970) Ferrozine – A new spectrophotometric reagent for iron. *Anal. Chem.* **42**(7), 779–781.

Tang M. and Liu Y. (2007) Re-evaluation of the equilibrium Fe isotope fractionation between $Fe^{3+}(H_2O)_6$ and $Fe^{3+}(H_2O)_6$ in aqueous solution. *Geochim. et Cosmochim. Acta Supplement* **71**, A1000 (abstr.).

Vollier E., Inglett P. W., Hunter K., Roychoudhury A. N. and VanCappellen P. (2000) The ferrozine method revisited: Fe(II)/Fe(III) determination in natural waters. *Appl. Geochem.* **15**(6), 785–790.

Welch S. A., Beard B. L., Johnson C. M. and Braterman P. S. (2003) Kinetic and equilibrium Fe isotope fractionation between aqueous Fe(II) and Fe(III). *Geochim. et Cosmochim. Acta* **67**, 4231–4250.

Weyer S. and Schwieters J. (2003) High precision Fe isotope measurements with high mass resolution MC-ICPMS. *Int. J. Mass spectrom.* **226**(3), 355–368.

Young E. D., Galy A. and Nagahara H. (2002) Kinetic and equilibrium mass-dependent fractionation laws in nature and their geochemical and cosmochemical significance. *Geochim. et Cosmochim. Acta* **66**, 1095–1104.

Associate editor: Thomas Chacko